Advanced Flame Spray Pyrolysis for Engineering Multifunctional Nanostructures

Subjects: Nanoscience & Nanotechnology

Contributor: Christos Dimitriou , Pavlos Psathas , Maria Solakidou , Yiannis Deligiannakis

Flame spray pyrolysis (FSP) is an industrially scalable technology that enables the engineering of a wide range of metal-based nanomaterials with tailored properties nanoparticles.

flame spray pyrolysis | complex assemblies | multifunctional nanomaterials/nanodevices

1. Introduction

Flame spray pyrolysis (FSP) is an industrially scalable technique for the synthesis of nanomaterials, which allows to produce many types of metal, or metal-oxide nanoparticles with tailored physicochemical properties [1]. At the heart of the FSP technology lies an intricate process design, involving precursor atomization, combustion, and nanoparticle formation [2]. This enables swift, single-step synthesis, eliminating the need for post-production treatments commonly required in other methodologies. Recent advancements have further elevated the prominence of FSP in the development of nanodevices, i.e., where nanoparticles can be in situ incorporated in complex functional arrays [3]. Thus, FSP not only revolutionizes nanomaterials' production but, with recent innovations, also paves the way for the next generation of nanodevices [4].

In the domain of nanotechnology, nanostructure synthesis represents a critical research area, encompassing a diverse range of methodologies alongside FSP. These alternative techniques, including, but not limited to, chemical vapor deposition, sol-gel processing, and electrospinning, offer unique properties in terms of particle size control, morphology, and chemical composition. The selection of an appropriate synthesis method is contingent upon a set of criteria closely related to the intended application of the nanostructures. Factors such as material versatility, environmental impact, synthesis time, and temperature range play a pivotal role in determining the suitability of a technique for specific applications, which vary from drug delivery systems to photovoltaic devices

1.1. Integration of Flame Spray Pyrolysis into the Technology Readiness Level (TRL) Scale for Nanomaterial Production

FSP stands out as an innovative and advanced methodology for the synthesis of nanomaterials, which highlights its vital role in producing a wide array of metal oxide nanoparticles with tailored morphologies and compositions [5]. Inherent in FSP, synthesis at elevated temperatures enhances both the crystallinity and physicochemical attributes of the nanoparticles. By adeptly adjusting operational parameters, such as precursor solution concentration, solvent type, flame temperature, oxygen-to-fuel ratio, and particle residence time in the flame zone, researchers

can effectively control the nanoparticle size, distribution, and phase composition. Regarding the technology readiness level (TRL) spectrum, FSP for device applications aligns with TRL 6–8 [6]. This placement signifies FSP's evolution beyond foundational laboratory research [1]. Given the adoption of FSP by certain industries, this positions FSP in the late stages of development and early stages of commercialization, placing it in the TRL 7–8 range (see **Figure 1**) [6].

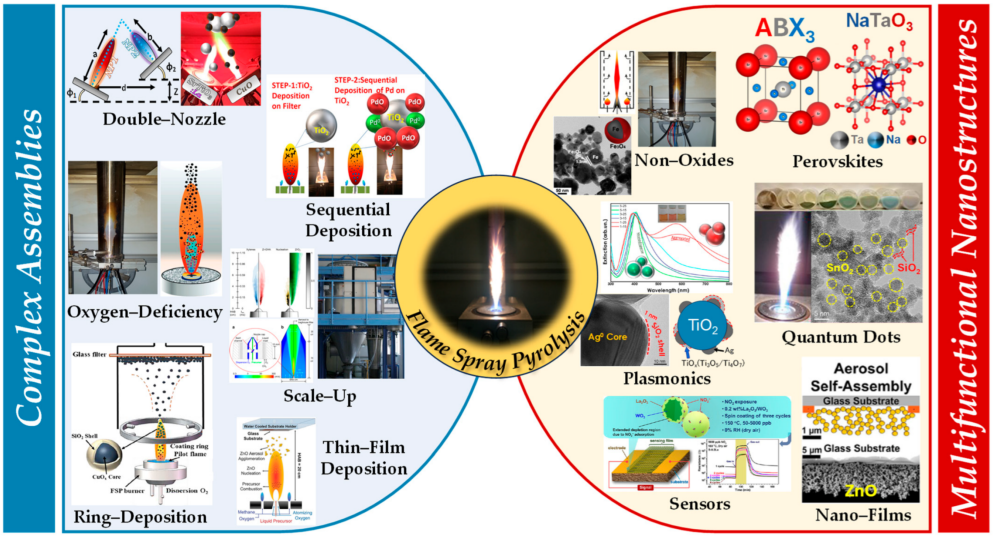

Figure 1. Figure illustrating the complex assemblies in flame spray pyrolysis (FSP). These include double-nozzle, sequential deposition, oxygen-deficiency process, ring deposition, sequential/thin-film deposition, and scale-up methods. The resultant advanced nanomaterials/nanodevices encompass perovskites, non-oxides, quantum dots, plasmonics, nanofilms, and sensors.

1.2. Process Design

The process design of FSP [7] begins with the preparation of a metal or metal-organic precursor solution, typically dissolved in an appropriate solvent. This solution undergoes atomization, often facilitated by a high-pressure nozzle, to form a fine spray of droplets [2]. Subsequent ignition of these droplets, often with the aid of an auxiliary flame, leads to the combustion of the solvent and the eventual decomposition of the metal precursors. Within this flame environment, characterized by elevated temperatures, the precursor decomposes, and metal or metal-oxide nanoparticles nucleate and grow [8]. The characteristics of the resultant nanoparticles—size, morphology, crystallinity, and phase composition—can be controlled by diligent choice of the metal precursor, its concentration in the solution, the solvent's nature, the atomization method, flame temperature, oxygen-to-fuel ratio, and the residence time of particles within the flame. Both inorganic and organic metal salts—including nitrates, acetates, and 2-ethylhexanoates—as well as metalorganic compounds such as acetylacetonates or alkoxides, serve as prevalent precursors [9]. These compounds are soluble in organic solvents, notably xylene (with a standard enthalpy change in combustion [10], $\Delta_c H^{\varnothing}_{298}$ = −4550 kJ mol^{-1}), toluene (−3910 kJ mol^{-1}), ethanol (−1376 kJ mol^{-1}), acetonitrile (−1256 kJ mol^{-1}), etc. Another pivotal aspect of the FSP design is its continuous mode of operation that enhances its scalability potential, making it an attractive proposition for industrial applications.

Furthermore, the high-temperature synthesis environment ensures rapid crystallization of particles, obviating the need for post-process annealing. Meierhofer et al. [1] delineated the relationship between temperature and process residence time during each phase of the droplet-to-particle formation, as represented by the red line in **Figure 2**a and the flame temperature profile in **Figure 2**b. At the nozzle's apex, temperature fluctuations range from 500 to 400 °C within the initial 10 µs. Adjacent to the capillary tip, the flame's core registers the peak temperatures, oscillating between 3500 and 2500 °C (**Figure 2**). At this juncture, the precursor solution vaporizes, initiating the nucleation of the primary particles. Following initial particle formation, particles fuse cohesively within the temperature range of 1700–600 °C during coagulation and sintering processes. Driven by Brownian motion, these particles collide and coalesce, forming larger entities. As the sintered particles move further through the flame and into cooler regions (<600 °C), they can stick together into agglomerates, forming loose clusters. This clustering is due to physical forces, such as van der Waals interactions. Subsequently, these agglomerates transform into aggregates, binding more firmly through chemical (covalent) bonds in the temperature range of 400–200 °C. The FSP setup typically comprises components like liquid atomizers, combustion chambers, flame torches, and substrate holders for potential direct deposition of nanoparticles.

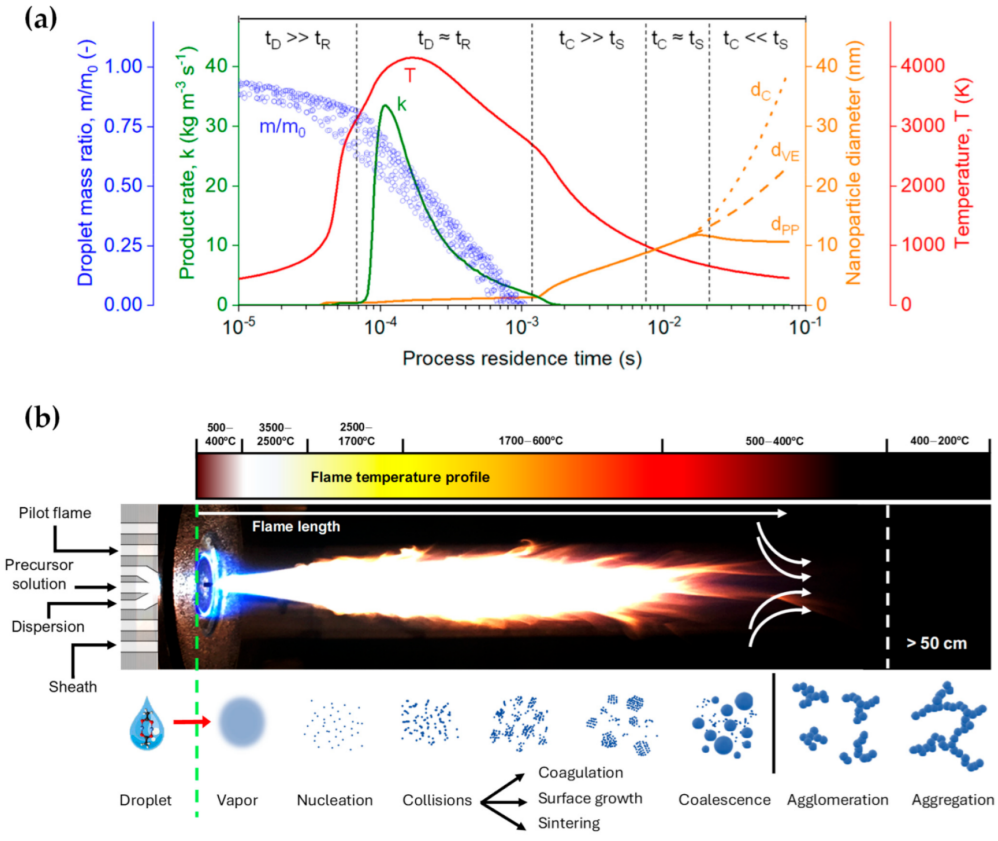

Figure 2. (**a**) Temporal scales in the fabrication of ZrO_2 nanoparticles via FSP. A time-evolving analysis encompasses the dynamics of the droplet mass ratio, the rate of product formation, nanoparticle diameter, and gas temperature, serving to demarcate distinct phases within the manufacturing process. (**b**) Visualization of actual FSP flame, depicting the synthesis parameters (pilot flame, precursor solution, dispersion, sheath gas). Concurrently, a graphical representation of the flame's temperature distribution, congruent with that depicted in (**a**),

is presented. Below the flame, a comprehensive elucidation of the droplet-to-particle transformation process in the production of nanoparticles is provided.

1.3. Recent Advancements in Product/Nanodevice Development

Figure 3 provides a chronological tracing of the literature articles related to FSP, highlighted by pertinent reviews. Introduced in the 1970s by Sokolowski et al. [11], FSP was utilized for synthesizing Al_2O_3 nanoparticles from an aluminum acetylacetonate precursor in a benzene-ethanol solution via an ultrasound nozzle. Despite the initial decline in interest, the technique was refined in the 1990s by Laine and colleagues at the University of Michigan [12] [13]. In a pilot-scale FSP reactor, a double-alkoxide (Mg-Al) precursor in an alcoholic solution was employed to yield spinel $MgAl_2O_4$ nanoparticles at rates between 50 and 100 g/h. Concurrently, scientists at Tampere University of Technology employed the FSP method for various metal oxide syntheses and conducted detailed optical diagnostics on the produced aerosols [14]. By the commencement of the 21st century, Pratsinis's team at the Swiss Federal Institute of Technology in Zürich further adapted FSP, highlighting its potential in catalytic material development [15].

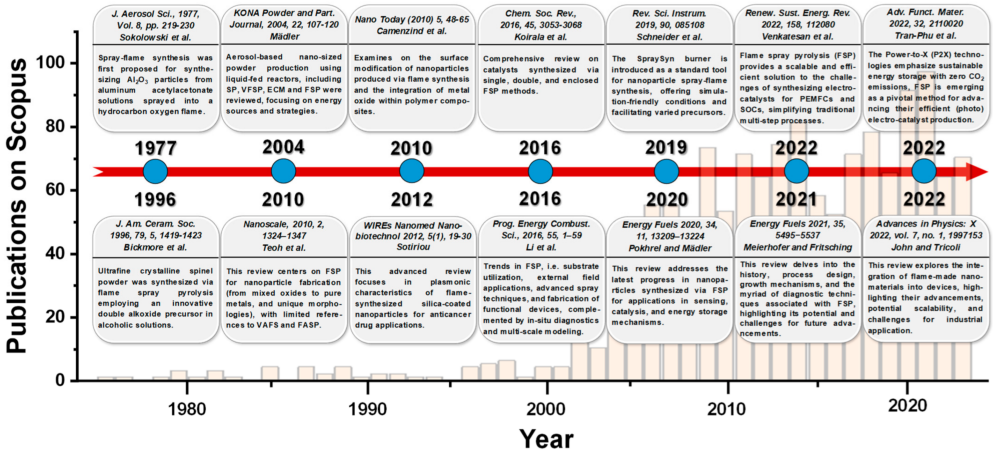

Figure 3. Timeline of the flame spray pyrolysis (FSP) technology, and some pertinent review articles. The bar graph depicts the annual publication frequency (1365 documents in total) from 1977 to 2023.

Mädler's review in 2004 [16] emphasized the increasing use of liquid-fed reactors for the aerosol-based synthesis of nano-sized powders. The rising interest in aerosol processes and the growing demand for various functional metal oxides have accelerated the R&D of these reactors. He examined four primary spray techniques: spray pyrolysis in a tubular reactor (SP), vapor flame reactor spray pyrolysis (VFSP), emulsion combustion method (ECM), and flame spray pyrolysis (FSP), comparing their energy sources and reaction mechanisms. He also outlined methods to produce consistent products and their specific applications [16]. In 2010, Teoh and colleagues [2] presented an exhaustive review focusing on FSP as a method for nanoparticle synthesis, spanning from mixed oxides to pure metals and encompassing specialized morphologies, such as core-shell structures, with minimal references to VAFS and FASP. Conversely, Camenzind and associates [17] delve into the surface functionalization of nanoparticles generated through flame synthesis and the incorporation of metal oxide within polymer composites.

Moreover, in 2013, Sotiriou [18] provided an in-depth review emphasizing the plasmonic properties of flame-synthesized silica-coated nanoparticles and their potential applications in anticancer drug delivery.

Koirala et al. in 2016 [19] conducted a thorough examination of catalysts produced through single, double, and enclosed FSP techniques. In the same year, Li and his colleagues [20] detailed advancements in FSP, encompassing substrate usage, applications of external fields, innovative spray methodologies, and the construction of functional apparatus, supplemented by in situ diagnostics and multi-scale simulations. In 2019, Schneider et al. [21] presented the SpraySyn burner as a benchmark instrument for the spray-flame synthesis of nanoparticles. This apparatus offers conditions amenable to simulation and accommodates a variety of precursors. One year later, Pokhrel and Mädler's review [22] outlined recent advancements in nanoparticles produced through FSP for sensing, catalysis, and energy storage applications, while Meierhofer and Fritsching in 2021 [1] provided a detailed analysis of FSP's historical context, design, growth mechanisms, and diagnostic methodologies, emphasizing its prospective opportunities and challenges.

Meanwhile, Venkatesan et al. [23] highlighted that FSP offers a scalable and proficient approach to address the complexities of electrocatalyst synthesis for polymer electrolyte membrane fuel cells (PEMFCs) and solid oxide cells (SOCs), streamlining conventional multistage procedures. In 2022, Tran-Phu et al. [24] presented a review on Power-to-X (P2X) technologies, underscoring the significance of sustainable energy storage with zero CO_2 emissions. Within this context, FSP is identified as a crucial technique for enhancing the production of efficient (photo)electrocatalysts. Ultimately, within that year, John and Tricoli's review [25] probed the particle formation mechanism, drawing insights from micro-explosions in single droplet experiments across diverse precursor–solvent pairs. The discussion emphasizes the importance of layer fabrication for industrial applications, including gas sensors, catalysis, and energy storage.

2. Engineering of Complex Nanoassemblies by Flame Spray Pyrolysis

2.1. Oxygen-Deficient FSP Process

The concept of oxygen-deficient synthesis can pertain to anoxic or reduced metal oxides. In the literature, these are referenced as M_KO_{L-x} where *K* and *L* are the stoichiometry coefficients that determine the stable crystal phase M_KO_L. In this terminology, x signifies the O-deficiency coefficient.

Here, for the sake of the discussion, researchers classify these materials in three cases:

[i] *O-vacancies generation with no change in the crystal phase*: lack of O atoms from the lattice, compared to the formal stoichiometry of the nominal crystal phase, with no modification of the crystal phase.

[ii] *Generation or reduced metal atoms with no change in the crystal phase*: lack of O atoms from the lattice can stabilize lower-oxidation states of the metal atoms.

Often, cases [i] and [ii] are interlinked since the reduction in individual metal atoms in the lattice can be triggered thermodynamically from the generation of one or more O-vacancies in its immediate vicinity.

[iii] *Stabilization of a reduced crystal phase* via *lack of O atoms*: certain O-deficient metal oxides can stabilize reduced phases. This occurs when a significant fraction part of the metal atoms is reduced. For example, magnetite Fe_3O_4, which contains one Fe^{2+} and two Fe^{3+}, can be formed from Fe_2O_3 (two Fe^{3+}) when 1/3 of the Fe^{3+}-atoms is reduced to Fe^{2+}. Further reduction in all Fe atoms to Fe^{2+} forms the FeO phase, while further reduction to Fe^0-atoms forms the metallic, zero-valent-iron material. Similarly, Cu_2O (SnO) is formed when all Cu^{2+} (Sn^{4+}) atoms in CuO (SnO_2) are reduced to the Cu^{1+} (Sn^{2+}) state.

The concept of using an oxygen-lean FSP was pioneered by Grass et al. to produce oxygen-deficient metal-oxide particles [26] by placing the FSP nozzle inside a glove box filled with inert nitrogen and regulating the intake of oxidizing gas as illustrated in **Figure 4**b,c. The dispersion gas mixture in the flame can shift from a CO_2/H_2O composition (representing traditional, oxidizing flames, see **Figure 4**a) to a $CO/H_2/H_2O$ mixture (under reducing conditions) [26]. Noble metal nanoparticles, including Pt, Au, Ag, and their alloys, can typically be produced even in oxygen-rich FSP, i.e., due to the thermodynamic preference of the metal state vs. the oxide state by the noble metal atoms. However, creating non-noble metals necessitates a reductive environment. When cobalt or bismuth organic precursors [27], such as cobalt(II)- and bismuth(III)-2-ethylhexanoate, are burned in a controlled atmosphere (with O_2 levels less than 100 ppm) and with a high fuel-to-oxygen ratio (see **Figure 4**b), it enables the swift production of pure Co and Bi metal nanoparticles, enhancing the conventional flame process. With this experimental setup, Stark et al. have explored the creation of metallic bismuth nanoparticles ensuring no soot formation [28]. While the reducing environment might be beneficial for producing metallic particles on a large scale [27][29], it comes with the risks of incomplete combustion [1]. In the case where the oxygen supply is further constrained, a fine carbonaceous layer tends to form on these metal nanoparticles [29][30]. Using this experimental setup, NiMo nanoalloys [31] and ZnS nanocompounds [32] have been reported.

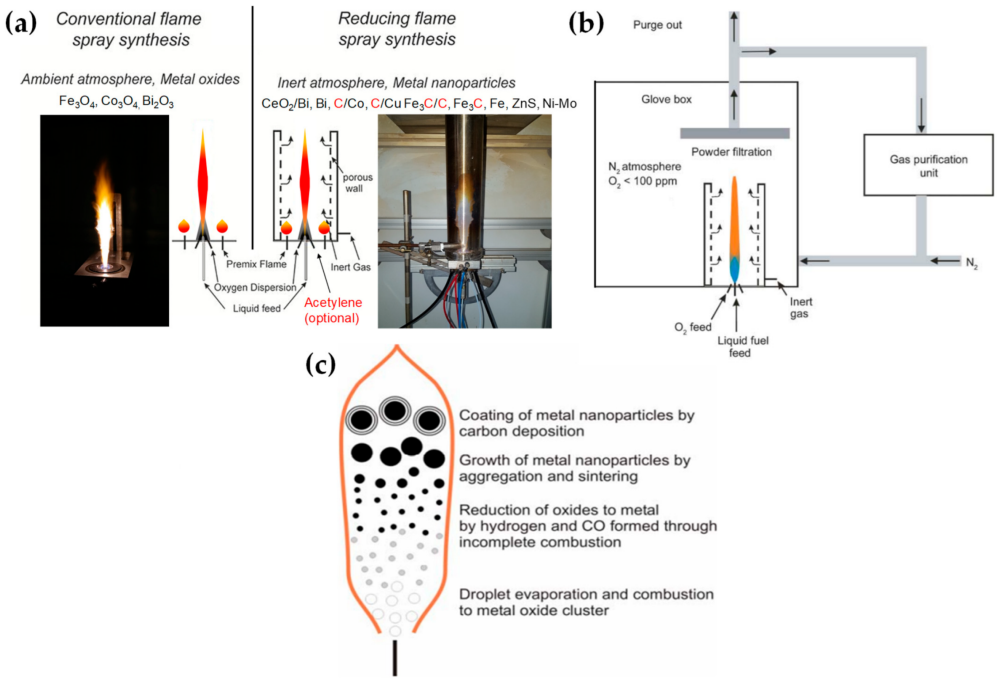

Figure 4. (**a**) Conventional FSP (left) and reducing FSP (right), where the anoxic flame is produced by in situ introduction of reducing dispersion gas, e.g., CH_4. (**b**) An anoxic FSP reactor, used by Stark, with the whole reactor enclosed in a glove box filled with an inert atmosphere. By adjusting the gas flow rates, it is possible to achieve highly reduced conditions (O_2 < 100 ppm). Used with permission of Royal Society of Chemistry from [27]; permission conveyed through Copyright Clearance Center, Inc. (**c**) Schematic depiction of the step-by-step transformation from precursor to oxide, metal, and carbon-coated metal nanoparticles during the reducing flame synthesis process: Initially, the precursor undergoes evaporation and combustion, resulting in oxide nanoparticles. These particles can then be further reduced to their metallic form by H_2 and CO. Throughout this procedure, the nanoparticles increase in size due to aggregation and sintering. By introducing acetylene, these metal nanoparticles can acquire a carbon coating layer.

Strobel and Pratsinis used an oxygen-deficiency FSP process [33] in order to synthesize Fe_2O_3, Fe_3O_4, and FeO nanoparticles. Their setup featured an FSP nozzle with a metal tube (4 cm in diameter and 40 cm in length) positioned directly above it (as shown in **Figure 4**b). Situated 20 cm above the FSP nozzle and angled at 45°, an internal mix spray nozzle was directed downward. This nozzle delivered deionized water at a rate of 10 mL/min, dispersed using 5 L/min of N_2. A different oxygen-deficiency FSP setup for the production of Fe_3O_4 nanoparticles may be the utilization of a laminar, inverse diffusion flame [34]. This method takes advantage of the properties of the inverse flame, created when an oxidizer is injected into a flow of surrounding fuel [35]. Contrary to conventional flame approaches, this setup ensures that the iron particle formation occurs in a predominantly reducing atmosphere. As illustrated in **Figure 5**a, the burner features two concentric brass tubes with specific outer diameters, enclosed within an 11.4 cm diameter acrylic chamber. This chamber is crucial for protecting the flame from ambient air, preventing additional particle oxidation and potential secondary diffusion flame formation due to excess fuel reacting with room air. The oxidizer, either pure O_2 or an O_2-Ar mixture, is released from the innermost tube and is encircled by a blend of fuel (methane or ethylene), argon, and iron precursor vapor. A N_2 flow enveloped the resulting inverse flame.

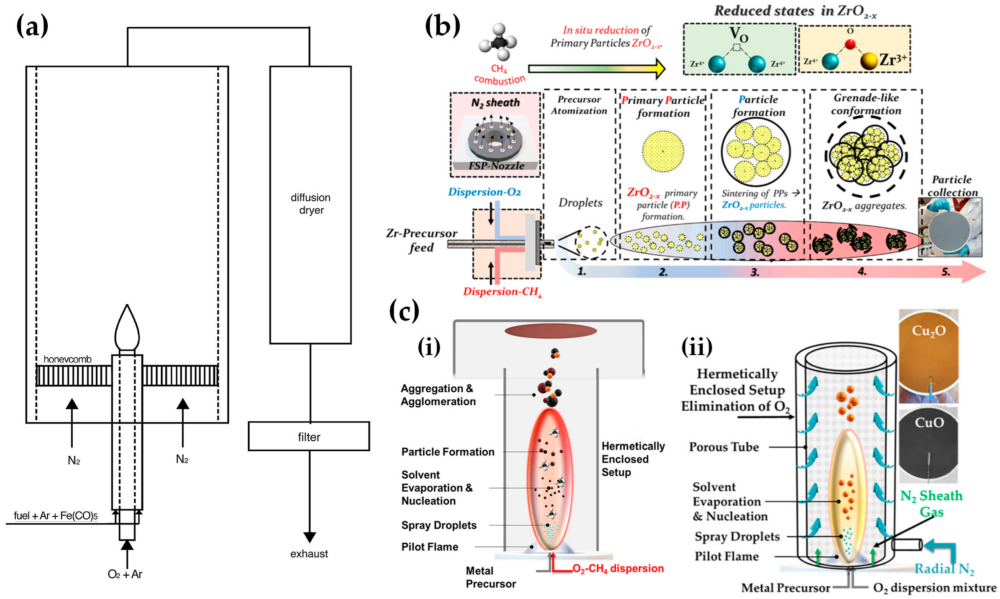

Figure 5. (**a**) Experimental setup of laminar, inverse diffusion flame stabilized on a burner for the synthesis of magnetic iron oxide nanoparticles with reduced oxidation state. (**b**) The concept of the novel anoxic FSP, for ZrO_{2-x} production. (**c**) (i) Schematic representation of anoxic FSP reactor used for the synthesis of $C@Cu_2O/Cu^0$ nanoparticles. (ii) Anoxic FSP reactor configuration utilized for creating CuO and Cu_2O nanomaterials.

Recently, researchers have exemplified a novel anoxic FSP process, to engineer ZrO_{2-x} (see **Figure 5**b) [36] and $C@Cu_2O/Cu^0$ (see **Figure 5**c) [37] nanoparticles. The anoxic FSP concept relies on the combustion of CH_4 in the dispersion gas. This introduces reducing agents that can modify the primary Zr particle by creating oxygen vacancies (V_O). XPS and EPR confirm that the increased dispersion of the CH_4 promotes the formation of oxygen vacancies [36]. A more complicated oxygen-deficiency FSP setup, which includes a dispersion feed consisting of {oxygen (O_2)–methane (CH_4)} mixture, in tandem with enclosed FSP flame with radial N_2, is necessary for the synthesis of non-graphitized carbon/Cu_2O/Cu^0 heterojunction (see **Figure 5**c) [37]. The modification in the dispersion gas mixture leads to increased temperatures and generates reducing agents for the controlled phase transformation from CuO to Cu_2O and Cu^0 (see **Figure 5**c).

2.2. Double-Nozzle FSP Configuration

In the case of mixed structures, e.g., heterojunctions, core-shell compositions, etc., the application of two FSP nozzles that operate in tandem offers advantages. Typical examples include the cases where a nanomaterial (NP1) and a cocatalytic nanomaterial (NP2) are combined. In the conventional single-nozzle FSP, a single precursor contains both the elements of nanomaterial (NP1) and nanomaterial (NP2) and produces the combined material in a single flame (see **Figure 6**a).

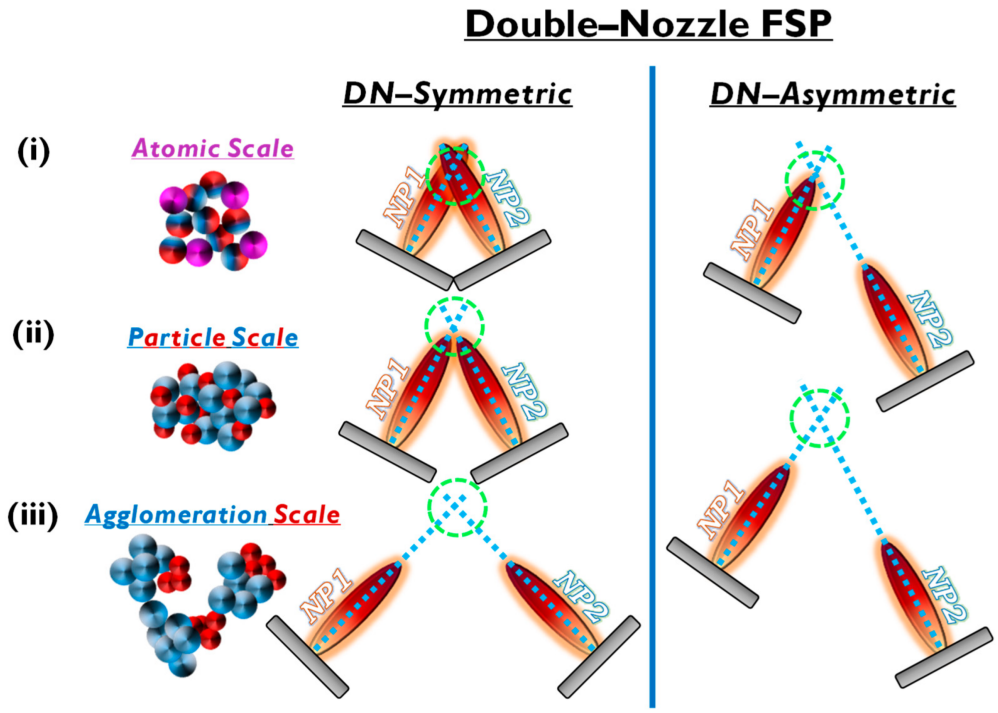

Figure 6. Symmetric and asymmetric DN-FSP configuration for two particle formation regarding the (**i**) atomic, (**ii**) particle, or (**iii**) agglomeration scale.

Double-nozzle FSP entails two independent spray flames, with the precursor of NP1 inserted in a different flame than NP2 (see **Figure 6**). This method unlocks several options for independent size control, mixing, and specific deposition for the two nanomaterials by altering the primary geometrical parameters of distance and intersection of the flames. As shown in **Figure 6**: (i) At a small flame-intersection distance, where the centers of the flames are in contact, the atoms are in the preliminary stages of crystallization, producing well-mixed particles, tending to be similar to the single-nozzle FSP. In this case, the second flame substantially increases the synthesis overall temperature. (ii) When the intersection occurs after the endpoints of the flames, the materials are well crystallized, resulting in well-mixed primary particles of NP1 and NP2. (iii) At increased intersection distance, the two materials mix at their sintering stage or bigger distances at the agglomeration stage.

Thus, by changing the geometrical disposition of the two flames via the parameters a, b, d, Φ_1, Φ_2, and Z (see **Figure 7**b), the symmetrical/asymmetrical DN-FSP configuration offers a versatile technology that allows for the control of composite configurations at different synthesis stages, i.e., at the atomic scale, at the particle scale, or the aggregate's scale (see **Figure 6**).

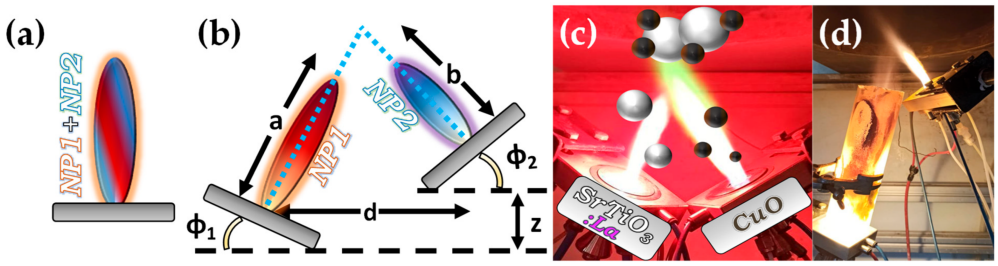

Figure 7. (**a**) Schematic example of SN-FSP where two precursors are mixed before being fed to the flame. (**b**) Geometry parameters of DN-FSP. (**c**) Example of a symmetrical DN-FSP, used for engineering of La-doped $SrTiO_3$, with surface deposition of CuO. (**d**) Example of asymmetrical DN-FSP.

Al_2O_3: DN-FSP was first implemented by Strobel et al. [38], producing in one nozzle Al_2O_3 and in the second nozzle $Pt/BaCO_3$, thus forming individual Al_2O_3 and monoclinic $BaCO_3$ nanoparticles. Increasing the internozzle distance delayed flame product mixing, increasing the crystallinity of $BaCO_3$. In contrast, the single-nozzle process yielded Al_2O_3 particles with amorphous Ba species. The two-nozzle process enhanced NO_x storage behavior, while the single-nozzle approach showed negligible NO_x retention [38]. Following this successful novelty method, a series of Al_2O_3-based articles were published, herein chronologically presented: Minnermann et al. [39] produced in one nozzle Al_2O_3 and in the other pure oxide or mixed CoO_x. Single flame synthesis is inadequate for producing an effective Al_2O_3/Co FT catalyst due to inadequate reducible cobalt oxide support particle size. The DN-FSP geometry significantly influences the resulting catalyst, yielding smaller alumina particles as the intersection distance increases, resulting in good adhesion of the two oxides and good stabilization. Høj et al. [40] produced Al_2O_3/CoMo by DN-FSP, and varying flame mixing distances (81–175 mm) minimized the formation of $CoAl_2O_4$,

detectable only at short flame distances. Notably, employing DN-FSP synthesis achieved superior promotion of the active molybdenum sulfide phase, potentially attributed to reduced $CoAl_2O_4$ formation, consequently enhancing Co availability for promotion. Schubert et al. [41], through DN-FSP, produced Al_2O_3/Co enhanced with Pt (0.03, 0.43 wt%) deposition in the first nozzle and other materials in the second nozzle. Noble metals enhance catalyst reducibility, yielding abundant metallic Co sites. Due to their high cost, optimizing synthetic strategies for low concentrations is essential. Regardless of the preparation approach, adding 0.03 wt% Pt significantly improves catalytic activity in CO_2 methanation, and 0.43 wt% Pt marginally increases the catalyst reduction. Using DN-FSP, Horlyck et al. [42] produced Al_2O_3/Co with Lanthanum doping (0–15 wt%). Increased La content and wider nozzle distance suppressed undesirable $CoAl_2O_4$ spinel phase, promoting easily reducible Co species. La addition enhanced carbon resistance, ensuring maximum methane conversions at 15 wt% La without catalyst deactivation or carbon formation. Stahl et al. [43] used DN-FSP to produce Co/Al_2O_3; in the nozzle of Al_2O_3, one additional particle—SmO_x, ZrO_x, or Pt—was formed contributing different cocatalytic effects, enhancing surface hydrogen or carbon oxide concentrations (see **Figure 8**a,b). All catalysts had consistent morphology with interconnected 12 nm alumina oxides and ~

8 nm cobalt oxides. For CO_2 methanation, Pt and zirconia proved optimal, aligning with Pt-enhanced H_2 adsorption and zirconia's higher CO_2 adsorption due to oxide sites with medium basicity.

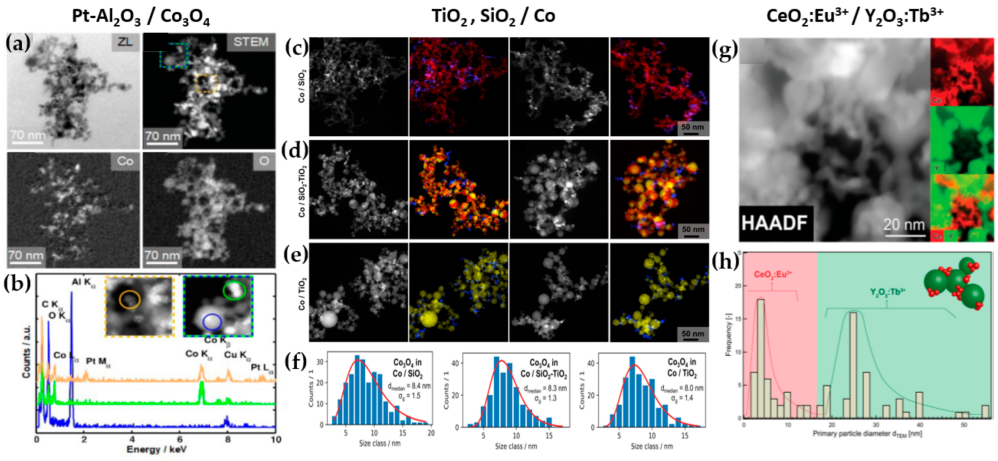

Figure 8. (**a**) TEM images revealing the local distribution of cobalt and oxygen for Pt-Al_2O_3/Co_3O_4, (**b**) EDX measurements for chemical composition. DN-FSP-prepared (**c**) SiO_2/Co, (**d**) SiO_2-TiO_2/Co, (**e**) and TiO_2/Co; left images show STEM-HAADF and right images show EDX mappings of the elements Co (blue), Si (red) and Ti (yellow). (**f**) Particle size distributions of Co_3O_4 for the materials SiO_2, SiO_2-TiO_2, and TiO_2. (**g**) STEM-HAADF of the nano-mixed CeO_2:Eu^{3+}/Y_2O_3:Tb^{3+} and its elemental mapping for Ce in red and Y in green, (**h**) d_{TEM} distribution of CeO_2:Eu^{3+} and Y_2O_3:Tb^{3+}.

TiO_2: Grossmann et al., through the utilization of DN-FSP, produced TiO_2 with deposited Pt particles [44]. Geometric configurations in DN-FSP strongly influenced Pt particle size and distribution on TiO_2. Larger intersection distances and smaller angles result in nonuniform large and broadly distributed Pt clusters on TiO_2. Conversely, smaller distances and larger angles enhance Pt dispersion and a uniform mixing, akin to single flame; however, DN-FSP

allows for individual tuning of compound particle sizes. Solakidou et al. produced {TiO_2-Noble metal} nanohybrids, with deposition of Pt^0, Pd^0, Au^0, or Ag^0 [45]. As shown, DN-FSP is superior vs. single-nozzle-FSP for finely dispersing noble metals on TiO_2 support, achieving a narrower size distribution [32]. DN-FSP promoted intraband states in TiO_2/noble metal, reducing the band gap. Efficient H_2 generation presented the following trend: Pt^0 > Pd^0 > Au^0 > Ag^0, in line with a higher Schottky barrier upon TiO_2 contact [32]. Gäßler et al. produced SiO_2, TiO_2, and SiO_2-TiO_2 mixture with DN-FSP deposition of Co_3O_4 (see **Figure 8**c–f) [46]: titania, comprising anatase and rutile phases, the SiO_2-TiO_2 mixed support, with separate anatase and silica phases. H_2O adsorption varies significantly based on the support: SiO_2 < SiO_2-TiO_2 < TiO_2. CH_4 formation rate increased with higher TiO_2 fractions, while CO formation rate peaked in the mixed support. Psathas et al. used DN-FSP to engineer heterojunctions of perovskite $SrTiO_3$ with deposited CuO nanoparticles (0.5 to 2 wt%) [47]. Higher CuO deposition led to larger $SrTiO_3$ particle sizes due to increased enthalpy from the second flame [22]. Scanning TEM depicted small CuO particles (<2 nm), mainly found on the surface of $SrTiO_3$. The dopant concentration significantly controlled the selective production of H_2 or CH_4 from H_2O/CH_3OH. CuO incorporation drastically shifted production to CH_4, achieving a rate of 1.5 mmol g^{-1} h^{-1} for the La:$SrTiO_3$/CuO catalyst (0.5 wt%) [47].

Other particles: Tada et al., using DN-FSP, produced a ZrO_2/CuO heterostructure [48]. Changing the geometrical parameters of DN-FSP altered the proportion of interfacial sites vs. copper surface sites. As active sites are primarily at the metal–oxide interface, ZrO_2/CuO with smaller CuO clusters exhibited higher activity in methanol synthesis via CO_2 hydrogenation. Gockeln et al., by a combination of DN-FSP and a lamination technique [49], synthesized in situ carbon-coated nano-$Li_4Ti_5O_{12}$ Li-ion battery electrodes. Li et al. synthesized $LiMn_2O_4$ spinel as a cathode material for Li-ion batteries via screening 16 different precursor–solvent combinations [50]. To overcome the drawback of capacity fading, the deposition of $AlPO_4$ (1–5%) via DN-FSP was homogeneously mixed with $LiMn_2O_4$. The optimal 1% $AlPO_4$ with $LiMn_2O_4$ demonstrated an energy density of 116.1 mA h g^{-1} at 1 C (one-hour discharge). Henning et al. used DN-FSP to engineer luminescent biosensors CeO_2:Eu^{3+}/Y_2O_3:Tb^{3+} [51]. CeO_2:Eu^{3+} nanoparticles (6 nm, 22 wt%) and Y_2O_3:Tb^{3+} nanoparticles (32.5 nm, 78 wt%) were shown to function as robust optical-based ratiometric H_2O_2 biosensors (see **Figure 8**g,h). Based on the collective effect, H_2O_2 caused significant luminescence quenching in CeO_2:Eu^{3+} nanocrystals, but Y_2O_3:Tb^{3+} nanoparticles were unaffected [30].

Asymmetric Double Flame: Lovell et al. utilized asymmetric-DN-FSP geometry to control the SiO_2 interaction with $Ce_{0.7}Zr_{0.3}O_2$ nanoparticles [52]. Tuning the intersection distance during DN-FSP (18.5 to 28.5 cm) prevented silica coating. Short intersection distances led to high surface-area silica encapsulating ceria-zirconia, while longer distances suppressed this encapsulation. The material at longer intersection distances, used as Ni support for dry methane reforming, showed enhanced oxygen storage capacity and basicity, yielding a highly selective catalyst. Psathas et al. used asymmetrical-DN-FSP-deposited NiO or Pt^0 nanomaterials on the surface of Ta_2O_5 or the perovskite $NaTaO_3$ [53]. Single-step synthesis of the smallest produced $NaTaO_3$ (<15 nm), with finely dispersed NiO or Pt^0 (<3 nm). $NaTaO_3$/NiO produced from FSP had half the photocatalytic hydrogen production than those from DN-FSP. Also, DN-FSP had a ten times higher yield than the conventional deposition of wet-impregnated NiO. Similar results were found for the photocatalytic efficiency of $NaTaO_3$/Pt^0, which was 30% more photocatalytically active than the conventional liquid-Pt photo-deposition method [36].

References

1. Meierhofer, F.; Fritsching, U. Synthesis of Metal Oxide Nanoparticles in Flame Sprays: Review on Process Technology, Modeling, and Diagnostics. Energy Fuels 2021, 35, 5495–5537.
2. Teoh, W.Y.; Amal, R.; Mädler, L. Flame Spray Pyrolysis: An Enabling Technology for Nanoparticles Design and Fabrication. Nanoscale 2010, 2, 1324–1347.
3. Ulrich, G.D. Special Report. Chem. Eng. News Arch. 1984, 62, 22–29.
4. Liu, S.; Mohammadi, M.M.; Swihart, M.T. Fundamentals and Recent Applications of Catalyst Synthesis Using Flame Aerosol Technology. Chem. Eng. J. 2021, 405, 126958.
5. Malekzadeh, M.; Swihart, M.T. Vapor-Phase Production of Nanomaterials. Chem. Soc. Rev. 2021, 50, 7132–7249.
6. Rsanchez. Technology Readiness Assessment Guide—DOE Directives, Guidance, and Delegations. Available online: https://www.directives.doe.gov/directives-documents/400-series/0413.3-EGuide-04a (accessed on 25 October 2023).
7. Workie, A.B.; Ningsih, H.S.; Shih, S.-J. An Comprehensive Review on the Spray Pyrolysis Technique: Historical Context, Operational Factors, Classifications, and Product Applications. J. Anal. Appl. Pyrolysis 2023, 170, 105915.
8. Teoh, W. A Perspective on the Flame Spray Synthesis of Photocatalyst Nanoparticles. Materials 2013, 6, 3194–3212.
9. Strobel, R.; Pratsinis, S.E. Flame Aerosol Synthesis of Smart Nanostructured Materials. J. Mater. Chem. 2007, 17, 4743.
10. CRC. Handbook of Chemistry and Physics, 95th ed.; Haynes, W.M., Ed.; CRC Press: Boca Raton, FL, USA, 2014; ISBN 978-1-4822-0867-2.
11. Sokolowski, M.; Sokolowska, A.; Michalski, A.; Gokieli, B. The “in-Flame-Reaction” Method for Al2O3 Aerosol Formation. J. Aerosol Sci. 1977, 8, 219–230.
12. Karthikeyan, J.; Berndt, C.C.; Tikkanen, J.; Wang, J.Y.; King, A.H.; Herman, H. Nanomaterial Powders and Deposits Prepared by Flame Spray Processing of Liquid Precursors. Nanostructured Mater. 1997, 8, 61–74.
13. Bickmore, C.R.; Waldner, K.F.; Treadwell, D.R.; Laine, R.M. Ultrafine Spinel Powders by Flame Spray Pyrolysis of a Magnesium Aluminum Double Alkoxide. J. Am. Ceram. Soc. 1996, 79, 1419–1423.
14. Tikkanen, J.; Gross, K.A.; Berndt, C.C.; Pitkänen, V.; Keskinen, J.; Raghu, S.; Rajala, M.; Karthikeyan, J. Characteristics of the Liquid Flame Spray Process. Surf. Coat. Technol. 1997, 90,

210–216.

15. Mädler, L.; Kammler, H.K.; Mueller, R.; Pratsinis, S.E. Controlled Synthesis of Nanostructured Particles by Flame Spray Pyrolysis. J. Aerosol Sci. 2002, 33, 369–389.
16. Mädler, L. Liquid-Fed Aerosol Reactors for One-Step Synthesis of Nano-Structured Particles. KONA Powder Part. J. 2004, 22, 107–120.
17. Camenzind, A.; Caseri, W.R.; Pratsinis, S.E. Flame-Made Nanoparticles for Nanocomposites. Nano Today 2010, 5, 48–65.
18. Sotiriou, G.A. Biomedical Applications of Multifunctional Plasmonic Nanoparticles. WIREs Nanomed. Nanobiotechnol. 2013, 5, 19–30.
19. Koirala, R.; Pratsinis, S.E.; Baiker, A. Synthesis of Catalytic Materials in Flames: Opportunities and Challenges. Chem. Soc. Rev. 2016, 45, 3053–3068.
20. Li, S.; Ren, Y.; Biswas, P.; Tse, S.D. Flame Aerosol Synthesis of Nanostructured Materials and Functional Devices: Processing, Modeling, and Diagnostics. Prog. Energy Combust. Sci. 2016, 55, 1–59.
21. Schneider, F.; Suleiman, S.; Menser, J.; Borukhovich, E.; Wlokas, I.; Kempf, A.; Wiggers, H.; Schulz, C. SpraySyn—A Standardized Burner Configuration for Nanoparticle Synthesis in Spray Flames. Rev. Sci. Instrum. 2019, 90, 085108.
22. Pokhrel, S.; Mädler, L. Flame-Made Particles for Sensors, Catalysis, and Energy Storage Applications. Energy Fuels 2020, 34, 13209–13224.
23. Venkatesan, S.; Mitzel, J.; Wegner, K.; Costa, R.; Gazdzicki, P.; Friedrich, K.A. Nanomaterials and Films for Polymer Electrolyte Membrane Fuel Cells and Solid Oxide Cells by Flame Spray Pyrolysis. Renew. Sustain. Energy Rev. 2022, 158, 112080.
24. Tran-Phu, T.; Daiyan, R.; Ta, X.M.C.; Amal, R.; Tricoli, A. From Stochastic Self-Assembly of Nanoparticles to Nanostructured (Photo)Electrocatalysts for Renewable Power-to-X Applications via Scalable Flame Synthesis. Adv. Funct. Mater. 2022, 32, 2110020.
25. John, A.T.; Tricoli, A. Flame Assisted Synthesis of Nanostructures for Device Applications. Adv. Phys. X 2022, 7, 1997153.
26. Grass, R.N.; Stark, W.J.; Athanassiou, E.-K. Reducing Flame Spray Pyrolysis Method for the Production of Metal, Non-Oxidic, Ceramic and Reduced Metal Oxide Powders and Nano-Powders, European Patent Office. European Patent EP1760043A1, 7 March 2007.
27. Grass, R.N.; Albrecht, T.F.; Krumeich, F.; Stark, W.J. Large-Scale Preparation of Ceria/Bismuth Metal-Matrix Nano-Composites with a Hardness Comparable to Steel. J. Mater. Chem. 2007, 17, 1485.

28. Grass, R.N.; Stark, W.J. Flame Spray Synthesis under a Non-Oxidizing Atmosphere: Preparation of Metallic Bismuth Nanoparticles and Nanocrystalline Bulk Bismuth Metal. J. Nanopart. Res. 2006, 8, 729–736.
29. Athanassiou, E.K.; Grass, R.N.; Stark, W.J. Large-Scale Production of Carbon-Coated Copper Nanoparticles for Sensor Applications. Nanotechnology 2006, 17, 1668–1673.
30. Grass, R.N.; Athanassiou, E.K.; Stark, W.J. Covalently Functionalized Cobalt Nanoparticles as a Platform for Magnetic Separations in Organic Synthesis. Angew. Chem. Int. Ed. 2007, 46, 4909–4912.
31. Athanassiou, E.K.; Grass, R.N.; Osterwalder, N.; Stark, W.J. Preparation of Homogeneous, Bulk Nanocrystalline Ni/Mo Alloys with Tripled Vickers Hardness Using Flame-Made Metal Nanoparticles. Chem. Mater. 2007, 19, 4847–4854.
32. Athanassiou, E.K.; Grass, R.N.; Stark, W.J. One-Step Large Scale Gas Phase Synthesis of Mn2+ Doped ZnS Nanoparticles in Reducing Flames. Nanotechnology 2010, 21, 215603.
33. Strobel, R.; Pratsinis, S.E. Direct Synthesis of Maghemite, Magnetite and Wustite Nanoparticles by Flame Spray Pyrolysis. Adv. Powder Technol. 2009, 20, 190–194.
34. Kumfer, B.M.; Shinoda, K.; Jeyadevan, B.; Kennedy, I.M. Gas-Phase Flame Synthesis and Properties of Magnetic Iron Oxide Nanoparticles with Reduced Oxidation State. J. Aerosol Sci. 2010, 41, 257–265.
35. Kumfer, B.M.; Skeen, S.A.; Axelbaum, R.L. Soot Inception Limits in Laminar Diffusion Flames with Application to Oxy–Fuel Combustion. Combust. Flame 2008, 154, 546–556.
36. Deligiannakis, Y.; Mantzanis, A.; Zindrou, A.; Smykala, S.; Solakidou, M. Control of Monomeric Vo's versus Vo Clusters in ZrO2−x for Solar-Light H2 Production from H2O at High-Yield (millimoles gr−1 h−1). Sci. Rep. 2022, 12, 15132.
37. Zindrou, A.; Belles, L.; Solakidou, M.; Boukos, N.; Deligiannakis, Y. Non-Graphitized Carbon/Cu2O/Cu0 Nanohybrids with Improved Stability and Enhanced Photocatalytic H2 Production. Sci. Rep. 2023, 13, 13999.
38. Strobel, R.; Mädler, L.; Piacentini, M.; Maciejewski, M.; Baiker, A.; Pratsinis, S.E. Two-Nozzle Flame Synthesis of Pt/Ba/Al2O3 for NOx Storage. Chem. Mater. 2006, 18, 2532–2537.
39. Minnermann, M.; Grossmann, H.K.; Pokhrel, S.; Thiel, K.; Hagelin-Weaver, H.; Bäumer, M.; Mädler, L. Double Flame Spray Pyrolysis as a Novel Technique to Synthesize Alumina-Supported Cobalt Fischer–Tropsch Catalysts. Catal. Today 2013, 214, 90–99.
40. Høj, M.; Pham, D.K.; Brorson, M.; Mädler, L.; Jensen, A.D.; Grunwaldt, J.-D. Two-Nozzle Flame Spray Pyrolysis (FSP) Synthesis of CoMo/Al2O3 Hydrotreating Catalysts. Catal. Lett. 2013, 143, 386–394.

41. Schubert, M.; Pokhrel, S.; Thomé, A.; Zielasek, V.; Gesing, T.M.; Roessner, F.; Mädler, L.; Bäumer, M. Highly Active Co–Al2O3 -Based Catalysts for CO2 Methanation with Very Low Platinum Promotion Prepared by Double Flame Spray Pyrolysis. Catal. Sci. Technol. 2016, 6, 7449–7460.
42. Horlyck, J.; Pokhrel, S.; Lovell, E.; Bedford, N.M.; Mädler, L.; Amal, R.; Scott, J. Unifying Double Flame Spray Pyrolysis with Lanthanum Doping to Restrict Cobalt–Aluminate Formation in Co/Al2O3 Catalysts for the Dry Reforming of Methane. Catal. Sci. Technol. 2019, 9, 4970–4980.
43. Stahl, J.; Ilsemann, J.; Pokhrel, S.; Schowalter, M.; Tessarek, C.; Rosenauer, A.; Eickhoff, M.; Bäumer, M.; Mädler, L. Comparing Co-catalytic Effects of ZrOx, SmOx, and Pt on COx Methanation over Co-based Catalysts Prepared by Double Flame Spray Pyrolysis. ChemCatChem 2021, 13, 2815–2831.
44. Grossmann, H.K.; Grieb, T.; Meierhofer, F.; Hodapp, M.J.; Noriler, D.; Gröhn, A.; Meier, H.F.; Fritsching, U.; Wegner, K.; Mädler, L. Nanoscale Mixing during Double-Flame Spray Synthesis of Heterostructured Nanoparticles. J. Nanopart. Res. 2015, 17, 174.
45. Solakidou, M.; Georgiou, Y.; Deligiannakis, Y. Double-Nozzle Flame Spray Pyrolysis as a Potent Technology to Engineer Noble Metal-TiO2 Nanophotocatalysts for Efficient H2 Production. Energies 2021, 14, 817.
46. Gäßler, M.; Stahl, J.; Schowalter, M.; Pokhrel, S.; Rosenauer, A.; Mädler, L.; Güttel, R. The Impact of Support Material of Cobalt-Based Catalysts Prepared by Double Flame Spray Pyrolysis on CO2 Methanation Dynamics. ChemCatChem 2022, 14, e202200286.
47. Psathas, P.; Zindrou, A.; Papachristodoulou, C.; Boukos, N.; Deligiannakis, Y. In Tandem Control of La-Doping and CuO-Heterojunction on SrTiO3 Perovskite by Double-Nozzle Flame Spray Pyrolysis: Selective H2 vs. CH4 Photocatalytic Production from H2O/CH3OH. Nanomaterials 2023, 13, 482.
48. Tada, S.; Larmier, K.; Büchel, R.; Copéret, C. Methanol Synthesis via CO2 Hydrogenation over CuO–ZrO2 Prepared by Two-Nozzle Flame Spray Pyrolysis. Catal. Sci. Technol. 2018, 8, 2056–2060.
49. Gockeln, M.; Pokhrel, S.; Meierhofer, F.; Glenneberg, J.; Schowalter, M.; Rosenauer, A.; Fritsching, U.; Busse, M.; Mädler, L.; Kun, R. Fabrication and Performance of Li4Ti5O12/C Li-Ion Battery Electrodes Using Combined Double Flame Spray Pyrolysis and Pressure-Based Lamination Technique. J. Power Sources 2018, 374, 97–106.
50. Li, H.; Erinmwingbovo, C.; Birkenstock, J.; Schowalter, M.; Rosenauer, A.; La Mantia, F.; Mädler, L.; Pokhrel, S. Double Flame-Fabricated High-Performance AlPO4/LiMn2O4 Cathode Material for Li-Ion Batteries. ACS Appl. Energy Mater. 2021, 4, 4428–4443.

51. Henning, D.F.; Merkl, P.; Yun, C.; Iovino, F.; Xie, L.; Mouzourakis, E.; Moularas, C.; Deligiannakis, Y.; Henriques-Normark, B.; Leifer, K.; et al. Luminescent CeO2:Eu3+ Nanocrystals for Robust in Situ H2O2 Real-Time Detection in Bacterial Cell Cultures. Biosens. Bioelectron. 2019, 132, 286–293.
52. Lovell, E.C.; Großman, H.; Horlyck, J.; Scott, J.; Mädler, L.; Amal, R. Asymmetrical Double Flame Spray Pyrolysis-Designed SiO2/Ce0.7Zr0.3O2 for the Dry Reforming of Methane. ACS Appl. Mater. Interfaces 2019, 11, 25766–25777.
53. Psathas, P.; Moularas, C.; Smykała, S.; Deligiannakis, Y. Highly Crystalline Nanosized NaTaO3/NiO Heterojunctions Engineered by Double-Nozzle Flame Spray Pyrolysis for Solar-to-H2 Conversion: Toward Industrial-Scale Synthesis. ACS Appl. Nano Mater. 2023, 6, 2658–2671.